Temperature dependence of carrier transport and resistance switching in Pt/$SrTi_{1-x}Nb_xO_3$ Schottky junctions

Jianyong Li,[1,*] Naoki Ohashi,[1,2,†] Hideyo Okushi,[2] and Hajime Haneda[2]

[1]*International Center for Material Nanoarchitectonics (NANA), National Institute for Materials Science (NIMS), 1-1 Namiki, Tsukuba, Ibaraki 305-0044, Japan*

[2]*National Institute for Materials Science, 1-1 Namiki, Tsukuba, Ibaraki 305-0044, Japan*

(Received 24 May 2010; revised manuscript received 28 November 2010; published 28 March 2011)

We investigated the temperature dependence of carrier transport and resistance switching of Pt/$SrTi_{1-x}Nb_xO_3$ Schottky junctions in the temperature range 80–400 K by measuring the current-voltage (*I-V*) characteristics and the frequency dependence of the capacitance-voltage (*C-V*) characteristics. The *I-V* curves displayed a high degree of hysteresis, known as the colossal electroresistance (CER) effect, and their temperature dependence showed an anomalous behavior, i.e., the magnitude of the hysteresis increased with decreasing *T*. The experimental results were analyzed by taking into account the temperature and electric-field dependence of the relative permittivity of $SrTi_{1-x}Nb_xO_3$ as well as the inhomogeneity of the Schottky barrier height (SBH) (a model in which two parallel current paths coexist in the Schottky barrier). It was confirmed that the observed *I-V* and *C-V* curves were well simulated by this model, thus indicating that the CER effects originated in the field emission current through different SBHs and at different locations of the Schottky junctions. Based on these results, we explain the mechanism of the CER effect qualitatively in terms of this model. For this purpose, we take into account the pinched-off effect caused by the small-scale inhomogeneity of SBH and the existence of deep levels as a result of defects and unintentional impurities in the depletion layer of the Pt/$SrTi_{1-x}Nb_xO_3$ Schottky junctions.

DOI: 10.1103/PhysRevB.83.125317 PACS number(s): 73.40.Ns, 73.40.Gk, 81.05.Hd

I. INTRODUCTION

Strontium titanate ($SrTiO_3$) and its related solid solutions have attracted considerable research interest because of their native dielectric and ferroelectric properties,[1–3] as well as their current transport properties after doping.[4,5] Recently, significant attention has been paid to niobium-doped strontium titanate ($SrTi_{1-x}Nb_xO_3$), because metal/$SrTi_{1-x}Nb_xO_3$ Schottky junctions exhibit reversible resistance switching between different states in their current-voltage (*I-V*) curves, a property known as the colossal electroresistance (CER) effect.[6–13] Similar behavior has been observed for various transition-metal oxides,[14–26] and several models that assume different conducting mechanisms have been proposed to explain these CER effects. Furthermore, integrated circuits of nonvolatile resistance random access memories based on the CER effect have been realized having $Pr_{0.7}Ca_{0.3}Mn_3$ (PCMO),[27] NiO,[28] and Cu_xO[29] as the active layers.

Recently, the mechanism of the CER effect in metal or metallic oxide/$SrTi_{1-x}Nb_xO_3$ Schottky junctions has been extensively studied from both the experimental and theoretical perspectives,[6–13] and the fundamental features of the effect have been clarified. However, several issues are unresolved and further experimental and theoretical investigations are obviously required for a more complete understanding of the CER effect. When considering the origin of the additional current paths across the Schottky junctions, a number of researchers have thought it highly possible that these current paths originate from inhomogeneity in the Schottky barrier height (SBH).[30–36] It has been pointed out that experimental data obtained from a number of metal/semiconductor (MS) interfaces are consistent with the assumption that SBH inhomogeneity is present.[34] A series of studies on SBH inhomogeneity in various MS systems have been carried out,[30–35] in which it has been shown that the presence of SBH inhomogeneity leads to a coherent explanation for many of the anomalies in the experimental results.[35] For metallic oxide/$SrTi_{1-x}Nb_xO_3$ Schottky junctions, Ramadan *et al.* discussed the *I-V* curves they observed in terms of SBH inhomogeneity,[37] but they did not discuss how this might be related to the CER effect. To elucidate the mechanism of the CER effect, it is important to clarify the relationship between the CER effect and SBH inhomogeneity.

It has been confirmed that the relative permittivity (ε_r) of the depletion layer of a metal/ $SrTi_{1-x}Nb_xO_3$ Schottky barrier strongly depends on the temperature (*T*) and electric field (*E*).[38–40] Suzuki *et al.*[39] and Yamamoto *et al.*[40] reported that the $\varepsilon_r(E,T)$ value of $SrTi_{1-x}Nb_xO_3$ is approximately given by the following relation:

$$\varepsilon_r(E,T) = \frac{b(T)}{\sqrt{a(T)+E^2}}, \tag{1}$$

where $a(T)$ and $b(T)$ are constant for a given *T* and are given by $a(T) = [b(T)/\varepsilon_r(E=0,T)]^2$ and $b(T) = 1.37 \times 10^{11} + 4.29 \times 10^9 T$ (V/cm).

Based on $\varepsilon_r(E,T)$, Susaki *et al.* simulated *I-V* curves for the temperature dependence (from 10 to 300 K) of their Au/$SrTi_{1-x}Nb_xO_3$ (0.01 wt %) Schottky junction.[41] They found that the permittivity of $SrTiO_3$ near the interface exhibited a *T* dependence that was the opposite to that observed in the bulk, which significantly reduced the barrier width. At low *T*, the tunneling current dominated the junction transport because of the narrowing of the barrier. Based on these results, they successfully explained the observed *T*-dependent reversal of the rectifying polarity in their sample.[41] In their report, however, the CER effect, that is, the hysteresis in the *I-V* curves, as in the results shown in Fig. 1, was not addressed at all. With regard to the CER effect, Shang *et al.* recently reported that the tunneling process of electrons through the

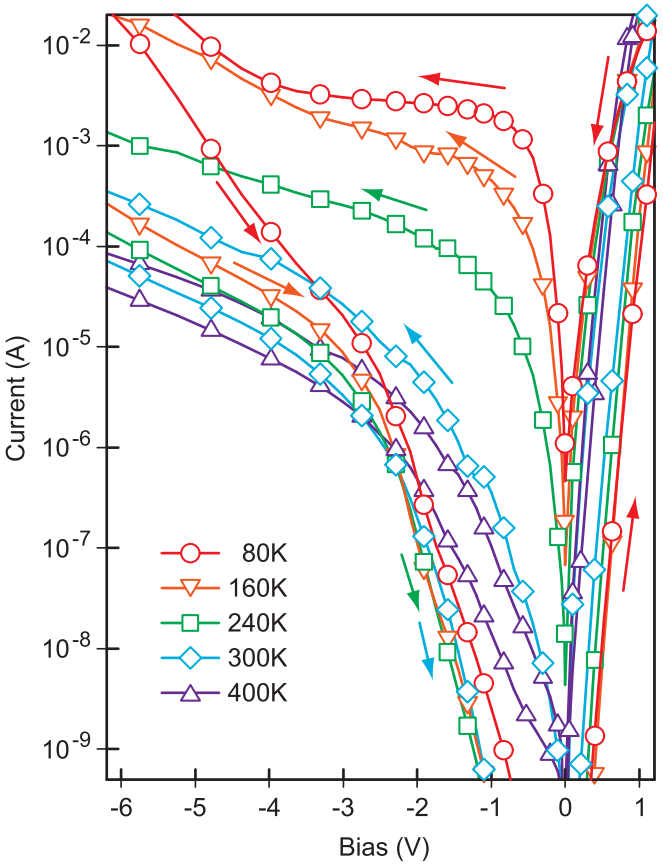

FIG. 1. (Color online) Temperature dependence of *I-V* curves of $Pt/SrTi_{1-x}Nb_xO_3$ (0.5 wt %) Schottky junction with thermal treatment surface at 1400 °C. Arrows indicate sweeping direction of applied bias.

junction remained dominant even in a high-T region from 293 to 454 K, and that it played an important role in the CER effect.[12] Thus, to elucidate the mechanism of the CER effect, it is important to gain a detailed understanding of the carrier transport properties of metal/ $SrTi_{1-x}Nb_xO_3$ Schottky junctions.

In this study, to understand the mechanism of the CER effect, we investigated the T dependence of the carrier transport properties of $Pt/SrTi_{1-x}Nb_xO_3$ Schottky junctions in the temperature range 80–400 K. We did this by measuring the current-voltage (*I-V*) characteristics and measuring-frequency (f_m) dependence of the capacitance-voltage (*C-V*) characteristics. The *I-V* curves clearly showed the CER effect, and their T dependence showed an anomalous behavior, i.e., the magnitude of the hysteresis increased with decreasing T. These *I-V* and *C-V* curves were analyzed by taking into account the temperature and electric field dependences of the relative permittivity of $SrTi_{1-x}Nb_xO_3$ and the SBH inhomogeneity. This is because the SBH of the $Pt/SrTi_{1-x}Nb_xO_3$ (0.5 wt %) Schottky junction is not uniform, and a large current flows through a local area with a low SBH region in the low-resistance state. The experimental results were well reproduced by simulations based on our model. Furthermore, on the basis of our model, we explain the mechanism of the CER effect qualitatively, taking into account the pinched-off effect caused by the small-scale inhomogeneity of SBH and the existence of non-negligible deep levels in the depletion layer of the Schottky junction.

II. EXPERIMENTAL PROCEDURE

We used commercially available 0.5-wt % Nb-doped $SrTiO_3$ single crystals. Hall measurements revealed that the free-carrier (electron) concentration was 2×10^{20} cm^{-3}, a value that remained constant within a temperature range T = 80–300 K. A 700-μm-diameter Pt electrode was deposited on the surface by dc sputtering, and an Ohmic Al electrode was formed on the back side of the crystal by vacuum evaporation. In general, the preparation of a semiconductor surface is crucial to the metal/semiconductor's junction properties. In our previous work,[13] we found that the CER effect of a $Pt/SrTi_{1-x}Nb_xO_3$ Schottky junction was strongly dependent on the preparation procedure for the $SrTi_{1-x}Nb_xO_3$ surface before the evaporation of Pt metal on that surface. In this study, we focused on a junction subjected to thermal treatment, in which the surface of the $SrTi_{1-x}Nb_xO_3$ was annealed at 1400 °C in air for 2 h, thereby achieving an atomically flat surface before the electrodes were deposited. We could obtain reproducible junction characteristics from such junctions, at least in a low applied voltage region. The *I-V* measurements were performed using a Keithley 237 source measure unit, while the *C-V* measurements were carried out using an Agilent 4284A LCR meter.

III. EXPERIMENTAL RESULTS

Figure 1 shows the T dependence of the *I-V* curves of the $Pt/SrTi_{1-x}Nb_xO_3$ (0.5 wt %) Schottky junction. Hysteresis in both the forward and reverse *I-V* curves, which corresponded to CER, were observed for all measurement temperatures (T = 80–400 K), although the *I-V* characteristics displayed the rectification characteristic of a conventional Schottky junction, which is similar to that of a metal/n-type semiconductor junction.[42] In the figure, the OFF current flows in a bias sequence from reverse to forward bias (R to F), while the ON current flows in a bias sequence from forward to reverse bias (F to R). In addition, the switching from OFF to ON occurs when the R to F bias sequence switches to the F to R sequence, and the switching from ON to OFF occurs when the F to R bias sequence switches to the R to F sequence. Furthermore, the T dependence of the hysteresis shows an anomalous behavior, i.e., the magnitude of the hysteresis increases with decreasing T. This phenomenon is quite different from that of a conventional Schottky junction in which the reverse current level generally decreases with decreasing T.[42]

Figure 2 shows the temperature (T = 80–400 K) and f_m dependence [f_m = (a) 1000 kHz, (b) 10 kHz, and (c) 0.1 kHz] of the *C-V* curve of the $Pt/SrTi_{1-x}Nb_xO_3$ (0.5 wt %) Schottky junction. The *C-V* curves at higher frequencies and lower temperatures showed conventional Schottky junction characteristics, in which the junction capacitance decreases with increasing reverse bias voltage.[42] However, in the case of lower frequencies and lower temperatures, the junction capacitance exhibits an anomalous behavior; the *C-V*

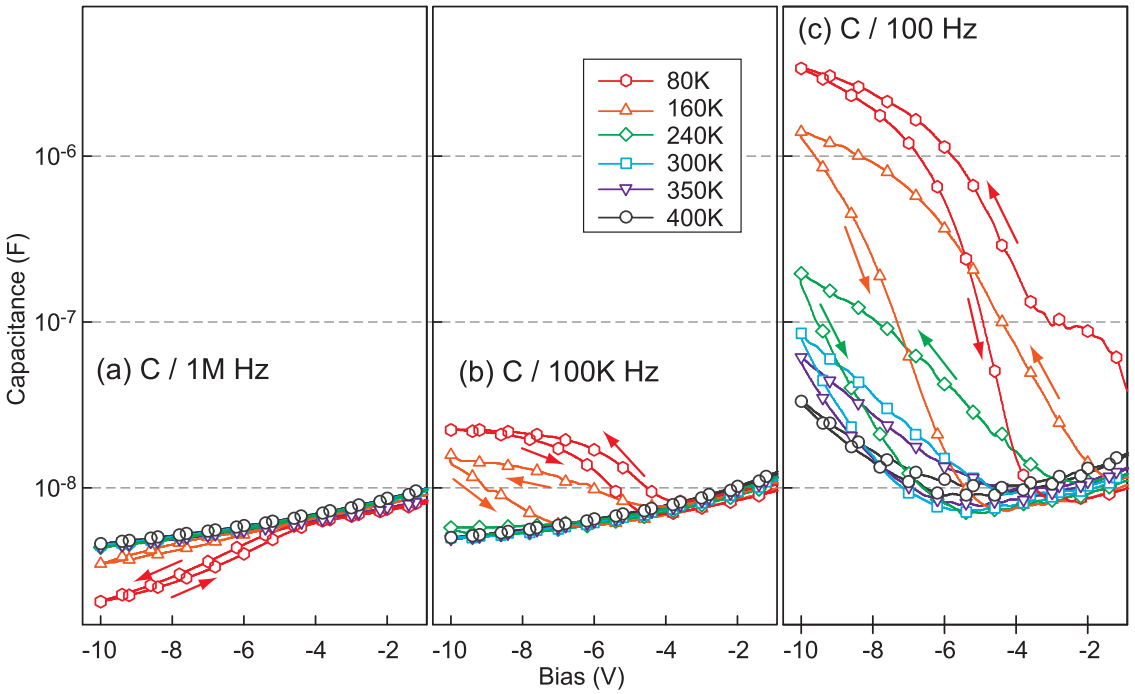

FIG. 2. (Color online) Temperature dependence of *C-V* curves for $Pt/SrTi_{1-x}Nb_xO_3$ (0.5 wt %) Schottky junction at fixed measurement frequencies of (a) 1000 kHz, (b) 10 kHz, and (c) 0.1 kHz.

curve assumes a U-shape with a high degree of hysteresis, as shown in the figure. In comparison to the *I-V* curve shown in Fig. 1, it appears that the hysteresis of the *C-V* curve corresponds to that of the *I-V* curves, namely, the CER effect. The real part of the complex admittance (G) at various temperatures measured with 0.1 kHz is shown in our previous report.[13] The variation of G with the bias was very similar to the *I-V* curves measured with dc current. Because the anomaly in the *C-V* plots was accompanied by an increase in the leakage current under a reverse bias, it has a correlation with the current leakage mechanism. On the other hand, the hysteresis was not obvious at low bias and high-frequency range, and indicates no essential change in the potential distribution of the Schottky barrier during resistance switching, a finding that is consistent with the previous results of Fujii *et al.*[7] and Shang and co-workers.[10,11]

IV. ANALYSIS

A. Calculation of *I-V* and *C-V* curves

In this work, in order to analyze the *I-V* curves in Fig. 1, we used the simulation methodology reported by Susaki *et al.*[41] We applied the unified transport theory of the Schottky junction developed by Fonash[43] to the present $Pt/SrTi_{1-x}Nb_xO_3$ (0.5 wt %) junction, in which the processes of thermionic emission, thermionic-field emission, and field emission are all included. On the calculations using this theory, the effective Richardson constant of $SrTiO_3$ was set to 156 A cm^{-2} K^{-2},[44] the effective mass of the electron in $SrTiO_3$ was set to $1.3 \times 9.11 \times 10^{-27}$ g, and the Schottky barrier potential was analytically determined as a function of the distance from the interface and applied voltage V_a by taking into account $\varepsilon_r(E,T)$ of the $SrTi_{1-x}Nb_xO_3$ junctions.[39,40] The bias dependence of barrier height (Φ_b) expressed by the following relationship was also considered in the calculations of *I-V* and *C-V* relationships:

$$\Phi_b = \Phi_{b0} + (1 - 1/n)Va. \quad (2)$$

Here Φ_{b0} is the barrier height at zero bias and n is the ideality factor of the diode.[39] These equations as well as the parameters for $SrTiO_3$ used in the calculation of the transmission probability of electrons through the Schottky barrier are essentially the same as those used in Refs. 39–41.

Moreover, we assume that the observed reverse currents are well explained by the field emission (FE) current through the barrier. Generally, the FE current at the reverse bias is determined by the probability of electrons tunneling through a barrier width (W_{FE}) measured at the position of the Fermi energy of the Schottky metal. Here, we consider the case where W_{FE} is smaller than the conventional depletion-layer width (W_d) of the Schottky barrier, as shown in Fig. 3. Thus W_{FE} can be correlated with W_d using Eq. (3),

$$W_d = W_{FE} + *W_d, \quad (3)$$

where $^*W_d$ is the remaining depletion layer width, as illustrated in Fig. 3. On calculation of *I-V* curves, we used Eq. (7) in Ref. 41. With this model, we need to introduce a series resistance (R_s) corresponding to the resistance for the electron drift current through $^*W_d$, even if the FE process is the dominant transport mechanism. In the case of conventional semiconductors, W_d, and consequently $^*W_d$, takes a small value of several nanometers when the FE current flows, because of a low relative permittivity ($\varepsilon_r \approx 10$). This is why the previous junction theories for conventional semiconductors did not consider R_s for $^*W_d$ when FE dominates the electron transport through the junction. In the case of a metal/$SrTiO_3$

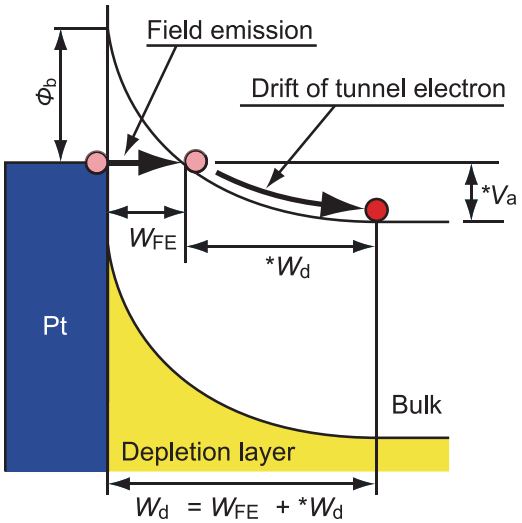

FIG. 3. (Color online) Model for field-emission current under reverse bias. The parameters W_d, W_{FE}, and ${}^*W_d$, are defined in the text.

interface, ${}^*W_d$ takes a large value and shows temperature dependence because the ε_r of $SrTiO_3$ is large (≈100–300 at 300 K) and strongly depends on the temperature and electric field. This is why we used the model shown in Fig. 3 and Eq. (3) and consider R_s for the drift current through ${}^*W_d$.

With this model, the magnitude of the drift current through ${}^*W_d$ (J_{drift}) is expressed by Eq. (4),

$$J_{drift} = q\mu n e \frac{{}^*V_d}{{}^*W_d}, \tag{4}$$

where q is the electric charge of the carrier, μ is the drift mobility, ${}^*V_d$ is the bias applied to ${}^*W_d$, and n_e is the effective carrier number for the drift current. Because $SrTi_{1-x}Nb_xO_3$ is a degenerated semiconductor, ${}^*V_d$ is approximately the same as the applied bias (V_a). Here, μ in the depletion layer is assumed to be the same as that in the bulk, and n_e is determined by the number of electrons passing through W_{FE} via the FE process (n_{FE}). From these assumptions, R_s can be roughly estimated as

$$R_s = \frac{{}^*V_d}{J_{drift}S} = \frac{{}^*W_d}{q\mu n_e S} \approx \frac{1}{q\mu n_{bulk}} \frac{n_{bulk}}{n_{FE}} \frac{{}^*W_d}{S} = \rho_{bulk} \frac{n_{bulk}}{n_{FE}} \frac{{}^*W_d}{S} = \rho_{FE} \frac{{}^*W_d}{S}, \tag{5}$$

where n_{bulk} and $_{bulk}$ are the carrier concentration and resistivity in bulk $SrTi_{1-x}Nb_xO_3$, S is the effective area of the electrode where the current flows, and n_{FE} is the resistivity in the depletion layer. Equation (5) implies that R_s takes a comparatively large value if n_{FE} is very low in comparison with n_{bulk} and ${}^*W_d$ is large. Because n_{FE} is proportional to the FE current, which increases exponentially with decreasing W_{FE},n_{FE} can take a wide range of values, from 0 to n_{bulk}(≈10^{20} cm^{-3}). As described later, for the actual case of the OFF state at $V_a = -3$ V and $T = 300$ K, we found $W_{FE} \approx 5$ nm and ${}^*W_d \approx 15$ nm and estimated that R_s was about 50 K Ω with $n_{FE} \approx 10^9$ cm^{-3} and $n_{bulk} \approx 10^{20}$ cm^{-3}. Thus R_s takes a comparatively large value at a low FE current. Note that this R_s is treated like the

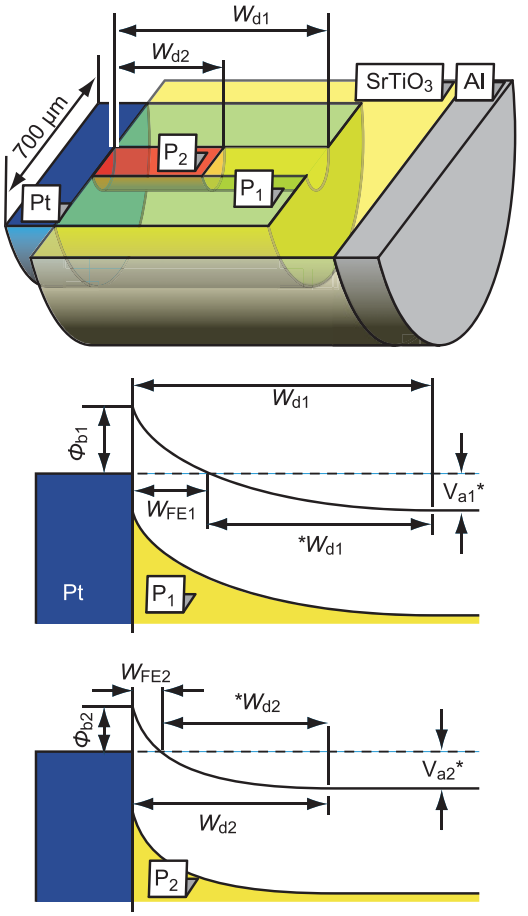

FIG. 4. (Color) Model assuming inhomogeneity of Schottky barrier height and presence of two parallel current paths through depletion layer.

conventional series resistance of a junction diode in the I-V curve fitting calculation described below.

To explain the conduction path of the OFF and ON states of CER, we introduce the factor of SBH inhomogeneity. That is, we assume that the SBH of the $Pt/SrTi_{1-x}Nb_xO_3$ (0.5 wt %) Schottky junction is not uniform, and that the ON current flows through a local area whose SBH is lower than the average SBH in the Schottky metal (Pt) electrode. In this model, two parallel current paths (P_1 and P_2) coexist in the Schottky barrier junction at equilibrium, as shown in Fig. 4. In this case, the current (I) at the applied bias (V) is given by

$$I = \frac{V_a}{R(V_a)} = \left(\frac{1}{R_1(V_a)} + \frac{1}{R_2(V_a)} \right) V_a, \tag{6}$$

where $R_1(V_a)$ and $R_2(V_a)$ are the effective resistances of P_1 and P_2, respectively, and are expressed by

$$R_1(V_a) = \frac{V_{a1}^*}{S_1 J_{FE}(V_{a1}^*)} + R_{S1} = \frac{1}{S_1} \left[\frac{V_{a1}^*}{J_{FE}(V_{a1}^*)} + \rho_{s1} {}^*W_{d1} \right],$$
$$R_2(V_a) = \frac{V_{a2}^*}{S_2 J_{FE}(V_{a2}^*)} + R_{S2} = \frac{1}{S_2} \left[\frac{V_{a2}^*}{J_{FE}(V_{a2}^*)} + \rho_{s2} {}^*W_{d2} \right], \tag{7}$$

and

$$V_{a1}^* = V_a - S_1 J_{FE}(V_{a1}^*) R_{S1},$$
$$V_{a2}^* = V_a - S_2 J_{FE}(V_{a2}^*) R_{S2}, \tag{8}$$

where S_i is the current-flow path area of the ith current path P_i, $J_{\rm FE}(V_{ai}^*)$ is the field-emission current density through P_i at effective bias (V_{ai}^*), and R_{si} is the effective series resistance for P_i defined by Eq. (5). Note that $J_{\rm FE}\left(V_{ai}^*\right)$ was calculated using unified theory[43] as mentioned above. In this model, as shown in Fig. 4, P_2 is represented by a single channel having junction area S_2. This illustration is used to simplify the description and does not mean that P_2 was a single channel in our samples. Here, we consider the areal fraction of S_1/S_2 as an essential parameter; namely, we may assume n channels with contact area S_i, with S_2 defined as $S_2 = \sum_i s_i$. Moreover, in Eq. (7), the series resistance of the bulk region and back side electrode of the junction is neglected because of the low resistivity of the bulk $SrTi_{1-x}Nb_xO_3$ (0.5 wt %), which is a degenerate semiconductor, and the low contact resistance at the $Al/SrTi_{1-x}Nb_xO_3$ junction.[7]

On the other hand, the capacitance at the $Pt/SrTi_{1-x}Nb_xO_3$ Schottky junction ($C_{\rm barrier}$) is obtained by taking into account $\varepsilon_r(E,T)$ of the junction as[39]

$$\frac{1}{C_{\rm barrier}} = \frac{n\sqrt{a(T)}}{SqN_D}\sinh\left(\frac{qN_D}{b(T)\varepsilon_0}W_d\right). \tag{9}$$

Absolutely, $a(T)$ and $b(T)$ in this equation represent field and temperature dependence of dielectric permittivity of $SrTiO_3$ expressed by Eq. (1) and W_d was calculated in Eq. (7) in Ref. 41.

To fit the calculated I-V and C-V curves to the experimental curves of the practical junctions, the following variable parameters were used: (i) $N_D(T)$, the temperature dependence of the space-charge density of the depletion layer; (ii) ϕ_{b0}, SBH at $V = 0$; (iii) n, the ideality factor of the junction; (iv) S, the area of the electrode through which the current flows; and (v) R_s, the effective series resistance of the junction diode caused by ${}^*W_d$. Note that we assumed that the junction capacitance was determined by the higher SBH region, while the lower SBH region was neglected because of its very small areal fraction.

B. Calculated *I-V* curves

Figure 5 shows the calculated T dependence of the current density (J) vs V_a curves under the conditions of $N_D = 1\times10^{20}\text{cm}^{-3}$, $\Phi_{b0} = 1.2$ eV, $n = 1$, and $R_s = 0$. Looking at the reverse bias region, the simulated curves well reproduced characteristic features found in the observed behavior. Actually, J increased with increasing reverse bias and decreasing T, except for the cases of the low bias region at $T > 300$ K, which were well reproduced in the simulated curves. The increase in J with reverse bias is mostly caused by the increase in the probability of electron field emission from the Pt electrode to $SrTi_{1-x}Nb_xO_3$. The assumption that the magnitude of the FE current is a function of $W_{\rm FE}$, rather than W_d, as mentioned in Sec. IV A, causes the increase in J with reverse bias, even though W_d increases with reverse bias. The anomalous T dependence of the I-V curves, i.e., the increase in I with decreasing T, is also reproduced by the assumption mentioned above, because both $W_{\rm FE}$ and W_d decrease with decreasing T because of the decrease in the $\varepsilon_r(E,T)$ of $SrTiO_3$ at the Schottky junction with decreasing T. On the other hand, in the forward bias region, as well as in the low reverse bias region at $T > 300$ K, the thermionic-field-emission current is still greater than the tunneling current with the parameters used for this simulation. Therefore the increase in J with increasing temperature in the forward bias range is reproduced in the assumed model.

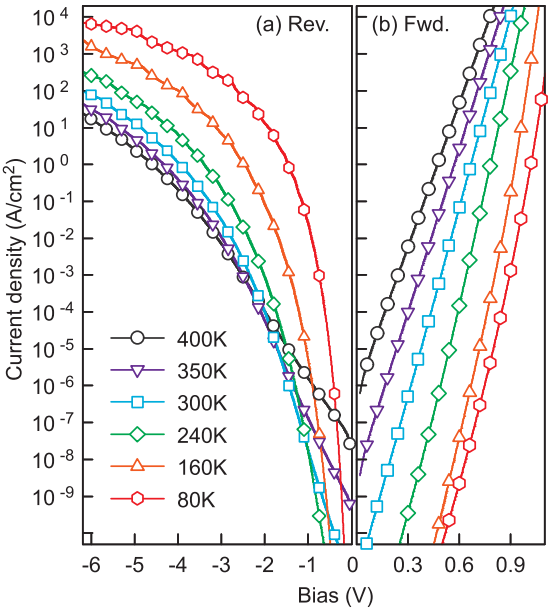

FIG. 5. (Color online) Temperature dependence of calculated J-V curves of metal/$SrTi_{1-x}Nb_xO_3$ Schottky junctions under conditions of $N_D = 1\times10^{20}$ cm^{-3}, $\Phi_{b0} = 1.2$ eV, $n = 1$, and $R = 0$.

We also calculated the N_D and Φ_{b0} dependence of the J-V curves. Figure 6(a) shows the N_D dependence (from 5×10^{20} to 1×10^{19} cm^{-3}) of the J-V curves under the conditions of $T =$ 300 K, $\Phi_{b0} = 1.2$ eV, $n = 1$, and $R_s = 0$, while Fig. 6(b) shows the Φ_{b0} dependence (from 0.3 to 1.8 eV) under the conditions of $T = 300$ K, $N_D = 1\times10^{20}$ cm^{-3}, $n = 1$, and $R_S = 0$. It should be noted that the calculated results in the figure do not correspond to the practical J-V curves, because the R_S caused by ${}^*W_d$ in Eq. (3) was neglected, i.e., $R_S = 0$, and the ideality factor of $n = 1$ was used in the calculation. The calculated J-V curves were strongly and sensitively dependent on both N_D and Φ_{b0}. That is, the J values vary superlinearly for small changes in N_D and Φ_{b0}. This is caused by the assumption that the J-V curves are mainly determined by the FE current as the result of the decrease in $W_{\rm FE}$, which is a function of N_D and Φ_{b0}. These large variations in the J-V curves for small changes in N_D and Φ_{b0} suggest that the large difference in the current levels between the ON and OFF states in CER is the result of changes in N_D and Φ_{b0} at a given T.

C. Fitting observed *I-V* curves

We tried to fit the calculated I-V curves to the experimental ones using the fitting parameters of S, n, $N_D(T)$, Φ_{b0}, and R_S, under the assumptions for the ON and OFF states described in Sec. IV A. Although N_D was treated as a constant in the simulations shown above, here it was treated as a T-dependent variable in order to obtain parameters for the best fit. The variation of N_D with temperature was justified by taking the transient behavior into account. The presence of defects and/or

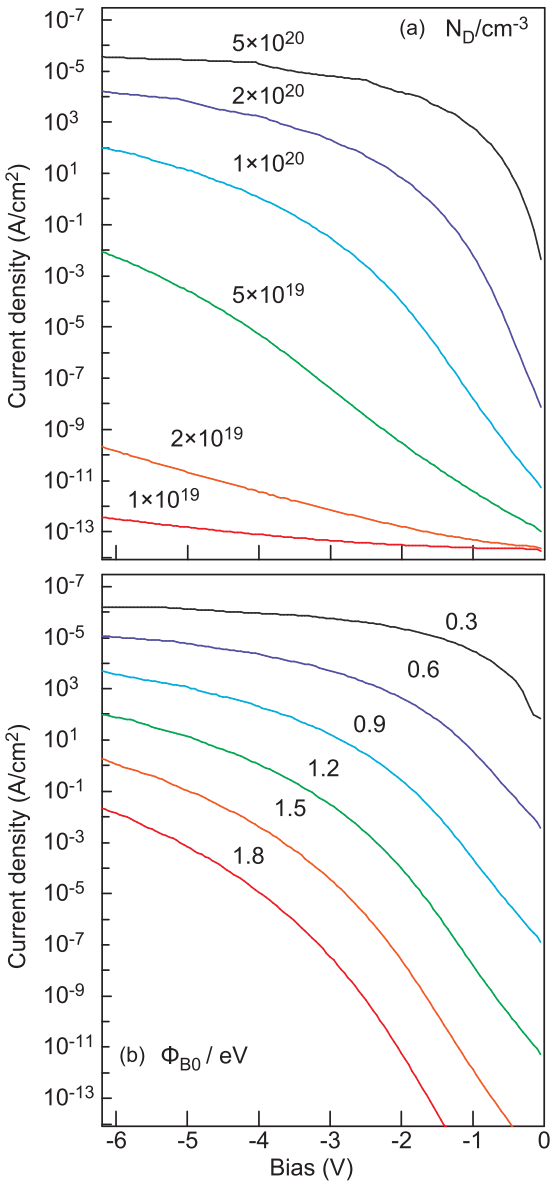

FIG. 6. (Color online) Calculated J-V curves: (a) N_D dependence (from 5×10^{20} cm^{-3} to 1×10^{19} cm^{-3}) under conditions of $T =$ 300 K, $\Phi_{b0} = 1.2$ eV, $n = 1$, and $R_s = 0$, and (b) Φ_{b0} dependence (from 0.3 to 1.8 eV) under conditions of $T = 300$ K, $N_D = 1 \times 10^{20}$ cm^{-3}, $n = 1$, and $R_s = 0$.

unintentional impurities causes the formation of localized states, and they affect the magnitude of N_D. At equilibrium, N_D is usually given as

$$N_{D0} = {}^*N_D - N_{T0}, \tag{10}$$

where N_{D0} is N_D at equilibrium, ${}^*N_D$ is the total donor density given by the summation of the shallow donor density (N_{Nb}) and deep donor densities, and N_{T0} is the total density of deep levels in the depletion layer at equilibrium. It should be noted again that this is the case of the equilibrium state and not the case of the transient state. The general I-V and C-V curves found by bias sweeping during certain limited measurement times are illustrated in Fig. 7. The electron trapping process takes place with a short time constant that is independent of both T and

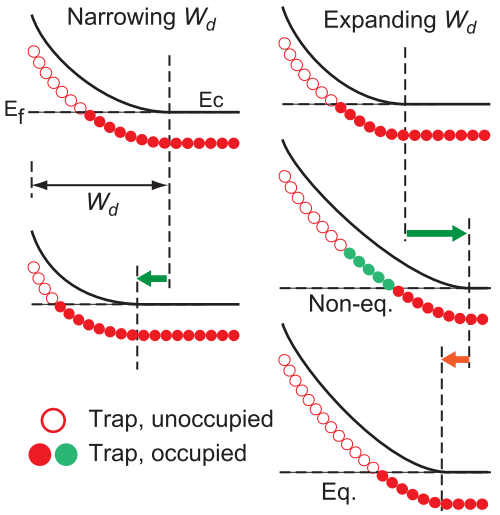

FIG. 7. (Color online) Schematic illustration of transient state for expansion and narrowing of depletion layer by varying reverse bias.

E_T, while the electron detrapping (thermal emission) process takes place with a time constant that varies as an exponential function of T and E_T, where E_T is the energy location of deep levels below the conduction-band minimum (E_c). For example, in the case of $E_T = 1$ eV at 200 K, the thermal emission time is on the order of 10^{14} s. This means that an electron trapped at such a deep level is not released during the practical measurement time (t_m) (e.g., t_m is on the order of 10^3–10^4 s in the case of the I-V measurement shown in Fig. 1). Thus in the case of low T with large E_T, N_D is not given by Eq. (10) during t_m but is generally given as a function of T and t as

$$\begin{aligned} N_D(T,t) = {}^*N_D - N_T(T,t) &= N_{D0} - [N_T(T,t) - N_{T0}] \\ &= N_{D0} - \Delta N_T(T,t), \end{aligned} \tag{11}$$

where $N_T(T,t)$ is the density of the occupied deep levels of the depletion layer and $\Delta N_T(T,t)$ is the net variation of $N_T(T,t)$ from the equilibrium value of N_{T0}. Because $SrTi_{1-x}Nb_xO_3$ has a wide band gap of 3.3 eV, and many deep levels with comparatively large E_T are present in $SrTi_{1-x}Nb_xO_3$,[45–47] it can be assumed that $\Delta N_T(t)$ always exists in the depletion region during t_m in a low-T regime such as $T < 240$ K. In such a case, N_D is given by a quasiequilibrium value, $N_D = N_{D0} - \Delta N_T$, where ΔN_T is the time average of $\Delta N_T(t)$ and ΔN_T increases with decreasing T. Based upon this argument, we set N_D as one of the temperature-dependent variable parameters in the fitting calculation.

In the actual fitting calculation, we focused on the I-V curves observed in the reverse bias region from 0 to −3 V, because reproducible I-V curves related to CER were observed in this bias region. We set the ideality factor of the diode as $n = 1.5$. Moreover, we assumed that the OFF-state current flowed in the entire electrode area ($S_{ON} = 4.41 \times 10^{-3}$cm^2), while we assumed that ON-state current flowed in the lower SBH region, P_2 in Fig. 4. The patch size of P_2 was set to $S_{ON} = 4.41 \times 10^{-5}$cm^2 (1% of the entire electrode area). The other fitting parameters used in the calculations are listed in Table I.

TABLE I. Fitting parameters used in calculation of *I-V* and *C-V* curves.

Temp. (K)	$N_D = N_b - N_T$ $\left(100^{20}\,\mathrm{cm}^3\right)$	SBH/eV ON	OFF
400	1.2	0.95	1.2
350	1.2	0.90	1.2
300	1.2	0.85	1.2
240	1.1	0.80	1.2
160	0.95	0.50	1.2
80	0.7	0.25	1.2
Temp. (K)	$Rs\ /k\Omega$ ON		OFF
400	100		200
350	75		200
300	50		200
240	10		150
160	1		100
80	0.5		50

As shown in Fig. 8, the observed T dependences of the *I-V* curves for both the ON and OFF states were well simulated by the calculations except for the case of the *I-V* curve for the OFF state at 80 K. The results presented in Fig. 8 confirmed (i) that the assumption described in Sec. IV A is valid, and (ii) that both carrier transports in the OFF and ON states of the CER effect are given by the unified transport theory of the Schottky junction,[43] and the OFF current flows through the entire electrode with a uniform high SBH, while the ON current flows through a small local area of the electrode with a low SBH.

D. Calculated *C-V* curves

First, we calculated the *C-V* curves of the simple Schottky barrier (C_{barrier}) given by Eq. (9). In Fig. 9, calculated *C-V* curves with different calculation conditions are compared with the observed *C-V* curves at $T = 300$ K. As shown here, the *C-V* curves for the reverse bias range 0 to -10 V, given by Eq. (9), are not strongly dependent on N_D or Φ_{b0}, in comparison to the *I-V* curves. Comparing the observed and calculated curves, the observed *C-V* curve, except for the U-shaped behavior [open symbols in Fig. 9(a)], could be reproduced by assigning parameters into Eq. (9). For example, the *C-V* curve measured with $f_m = 1$ MHz at 300 K could reproduced by a set of parameters as $N_D = 1.2 \times 10^{20}\mathrm{cm}^{-3}$, SBH $= 0.95$ eV, $S = 4.41 \times 10^{-3}$ cm^2, and $n = 2.2$. Note that the n value for reproduction of *C-V* plots ($n = 2.2$) is slightly larger than that used for the simulation of *I-V* curves ($n = 1.5$).

V. DISCUSSION

A. Validity of fitting parameters

In the simulations described above, we used $S_{\mathrm{OFF}} = 4.41 \times 10^{-3}$ cm^2 (the entire electrode area) for the OFF state of the *I-V* curves and the *C-V* curves, $S_{\mathrm{ON}} = 4.41 \times 10^{-5}$ cm^2 (1% of electrode area) for the ON state, $n = 1.5$ for all of the *I-V* and *C-V* curves, and the temperature-dependent parameters N_D, Φ_{b0}, and R_S that are listed in Table I. Here, we discuss the validity of using these fitting parameters.

1. *S and Φ_{b0} (SBH inhomogeneity)*

According to the basic concept of SBH inhomogeneity, there are two cases with different SBHs, depending on the size of the domain. The first is the case of "large-scale-inhomogeneity" (LS-IHG), where the dimensions of domains with different local SBHs were much larger than W_d. The other is the case of "small-scale inhomogeneity" (SS-IHG), where the dimensions of the domains with different local SBHs were comparable to or smaller than W_d. In the case of LS-IHG, domains with different local SBHs are electrically independent, and the total junction current is simply the sum of the currents flowing through all of the individual domains.[34,35] In the situation discussed in Refs. 34 and 35, the apparent SBH decreased and the ideality factors increased with decreasing T, depending on the standard deviations of the distribution functions.[36] On the other hand, in the case of SS-IHG, the conduction path for domains with an originally lower SBH was modulated (termed "pinched-off") to be determined by a higher potential (potential at "saddle point") than the original low SBH by the presence of a high SBH in close proximity.[35] In such cases, the current flows through the entire electrode of the Schottky junction, showing an apparently uniform SBH with weak temperature dependence.

The simulation results in Table I indicate that $\Phi_{b0} = 1.2$ eV for all T and S_{OFF} was given by the entire area of the electrode for the OFF state, while Φ_{b0} varied from 0.95 to 0.25 eV with decreasing T for the ON state, with a smaller area of S_{ON} than S_{OFF}. Furthermore, the result for $\Phi_{b0} = 1.2$ eV is nearly the same as the difference between the work functions of Pt and $SrTi_{1-x}Nb_xO_3$.[48] The temperature-independent Φ_{b0} in the OFF state strongly suggests that the degree of spatial fluctuation for an original low SBH is the case of SS-IHG, and that the pinched-off effect occurs in front of a patch with a low SBH.[35] On the other hand, the strong T dependence of Φ_{b0} in the ON state agrees well with the case of LS-IHG.[36] From this result, the comparatively large value of $S_{\mathrm{ON}} = 10^{-5}$–$10^{-4}$ cm^2 (1% of entire electrode area) can be considered to be the total area of the individual patches with the low SBH. Thus the values of Φ_{b0} and S for the OFF state determined by simulation are well explained by the SS-IHG model, while those for the ON state are explained by the LS-IHG model. This difference in the degree of spatial fluctuation between the OFF and ON states will be described in terms of the CER mechanism later.

It should be noted that the result of $S_{\mathrm{ON}} = 10^{-5}$–$10^{-4}$ cm^2 is still smaller than S_{OFF} by two orders of magnitude (1%), which indicates the formation of localized conduction path in the ON state. This result, as well as the results in which the junction capacitances C_{barrier} of the ON and OFF states measured at a high frequency of 1000 KHz were nearly the same as each other, as shown in Fig. 2, indicates no essential change in the potential distribution of the Schottky barrier during resistance switching as mentioned in the last part of Sec. III.

2. *n*

To fit the practical *I-V* and *C-V* curves, we need to introduce the ideality factor n of the Schottky barrier diode. The n

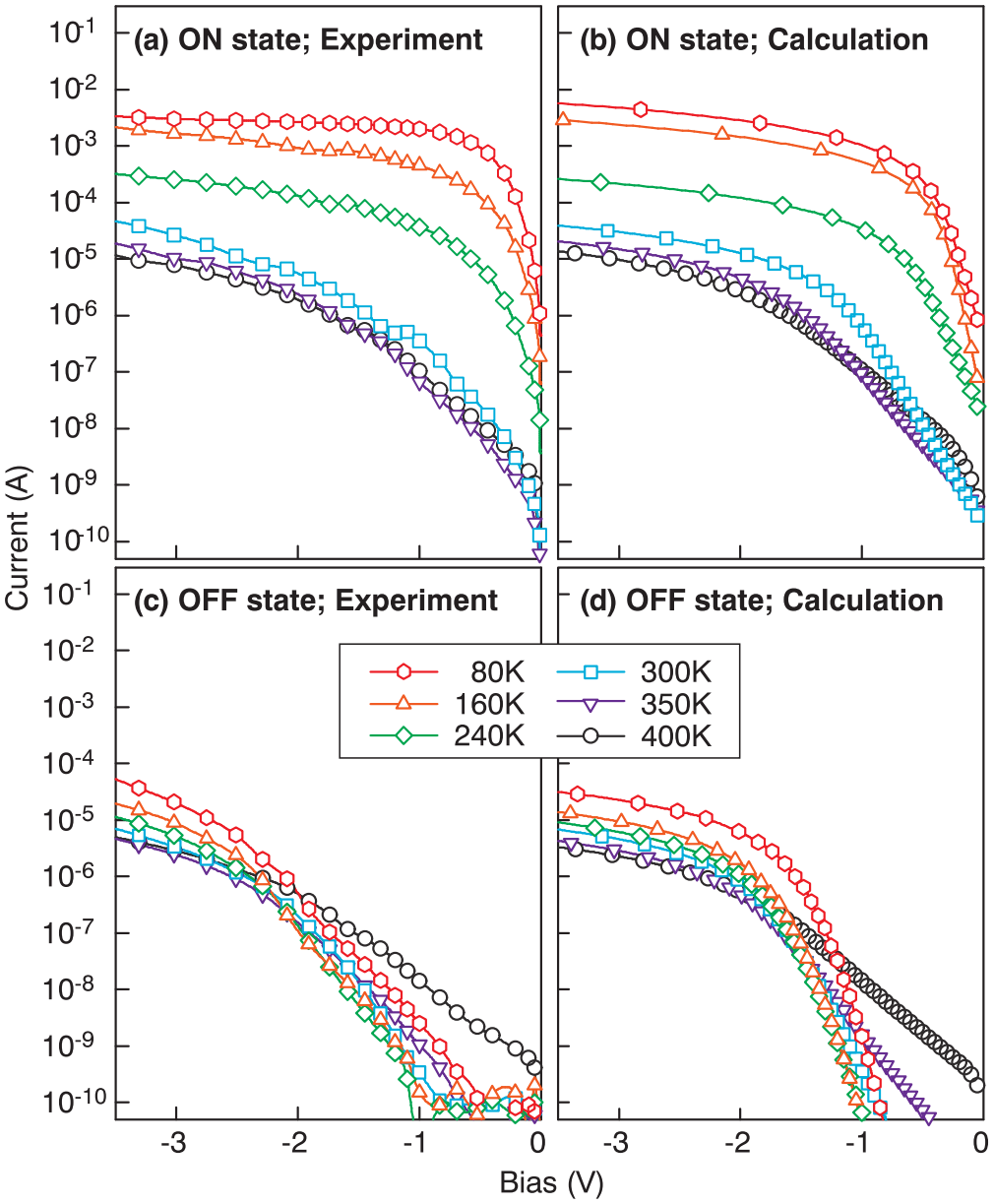

FIG. 8. (Color online) Temperature dependence of experimental and calculated (simulated) *I-V* curves of $Pt/SrTi_{1-x}Nb_xO_3$ (0.5 wt %) Schottky junction for both OFF and ON states of CER effect.

value is usually related to barrier lowering by the applied bias through Eq. (2). If Eq. (2) can be applied to the $Pt/SrTi_{1-x}Nb_xO_3$ junction, n is also related to C_{barrier} through Eq. (9). Though at present it is an open question as to whether Eq. (2) can be applied to the $Pt/SrTi_{1-x}Nb_xO_3$ junction, we used Eq. (2) in the fitting calculation, as described in Sec. IV A. Experimentally, n is deduced from the *I-V* curves in the forward bias region, taking a value of around 1.5 at 300 K and increasing with decreasing T. On the other hand, an n of around 1.5 is obtained from the fitting results of the *I-V* curve using Eq. (2), and $n = 2.1$ or more from the simulation results for the *C-V* curve using Eq. (9) [see Fig. 9(b)]. Such a discrepancy in the n values may originate from the use of Eq. (2). The actual simulation results, however, are not significantly affected by the discrepancy in the n values at each temperature. Therefore in the fitting calculations shown in Fig. 8, we set $n = 1.5$ as a constant for T, as a reasonable value for the present Schottky junctions.

3. N_D

The result of $N_D = N_{D0} = 1.2 \times 10^{20}$ cm^{-3} at 300 K nearly equals the carrier concentration (2×10^{20} cm^{-3}) determined by the Hall effect measurement at room temperature for the $SrTi_{1-x}Nb_xO_3$ (0.5 wt %) sample. The trend of the T dependence of N_D can, with good reason, be attributed to the existence of deep levels, as discussed in Sec. IV C. The result of $N_D = 7 \times 10^{19}$ cm^{-3} at 80 K indicates that N_{D0} is reduced by more than 40% by the electron-trapped deep levels, which indicates that a deep level density of more than 10^{19} cm^{-3} must exist in the $SrTi_{1-x}Nb_xO_3$ (0.5 wt %). Such a high density of defects and/or impurities acting at deep levels may be incorporated into the $SrTi_{1-x}Nb_xO_3$ (0.5 wt %), along

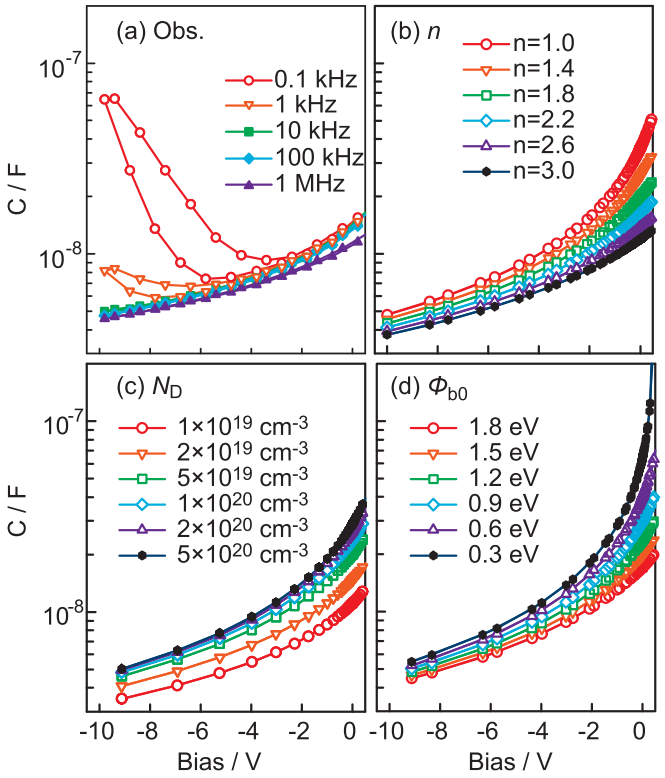

FIG. 9. (Color online) Observed (a) and calculated (b)–(d) C-V curves: (a) measured at 300 K. (b) n dependence (from 1 to 3) of C-V curves under conditions of $T = 300$ K, $N_D = 1 \times 10^{20}$ cm^{-3}, and $\Phi_{b0} = 1.2$ eV, (c) N_D dependence (from 5×10^{20} cm^{-3} to 1×10^{19} cm^{-3}) under conditions of $T = 300$ K, $\Phi_{b0} = 1.2$ eV, and $n = 1.5$, and (d) Φ_{b0} dependence (from 0.3 to 1.8 eV) under conditions of $T = 300$ K, $N_D = 1 \times 10^{20}$ cm^{-3}, and $n = 1.5$.

with the high density of Nb atoms, e.g., a complex of a vacancy and an Nb atom.

4. R_S

The simulation results indicate that the R_S of the OFF states (R_{SOFF}) decreased from 200 to 50 K Ω with decreasing T for $T < 300$ K, while the R_S of the ON states (R_{SON}) decreased from 100 to 0.5 K Ω with decreasing T at all measurement temperatures. These T dependences of R_S in both the OFF and ON states are consistent with the values estimated using Eq. (5), which gives rough values of R_S, as described in Sec. IV A. For example, in the case of the OFF state ($\Phi_{b0} = 1.2$ eV, $N_D = 1.2 \times 10^{20}$ cm^{-3} at 300 K) under a reverse bias of −3 V, W_{FE} and $^*W_d$ are calculated to be 5 and 15 nm, respectively, using Eqs. (5) and (7) in Ref. 41, and a value of about 10^9 cm^{-3} is obtained for n_{FE} using the results in Fig. 5. Next, considering that $\rho_{bulk} \approx 2 \times 10^{-3}$ Ω cm and $n_{bulk} \approx 2 \times 10^{20}$ cm^{-3} for the present bulk $SrTi_{1-x}Nb_xO_3$ and $S = 4.4 \times 10^{-3}$ cm^2, we obtain $R_S = 100-1000$ K Ω, which is consistent with the simulation results.

B. Mechanism of CER effect

1. Carrier transport in OFF and ON states

As shown in Fig. 8, we successfully simulated the experimental I-V curves. From these good simulation results, we reached the following conclusion: Except for the OFF current in the forward bias region, in which the thermionic-field-emission current mainly flows, both the OFF and ON currents originate from the FE current, and the difference between the OFF and ON states is caused by SBH inhomogeneity.

In most previous models of the CER effect, the opening/closing of the current path for the ON state has generally been considered, and the conduction mechanism for the ON state has been distinguished from the transport mechanism for the OFF state.[6–26] For example, Fujii *et al.* proposed a resonant tunneling current through the trapping state in the depletion layer as a conduction path existing only for the ON state.[7] However, the present results indicate that the carrier transport in both the ON and OFF states can be explained by the field-emission mechanism through the Schottky barrier. Thus although only a unified transport theory for Schottky junctions is considered for both the ON and OFF states, with the assumption of a lower SBH region, P_2 in Fig. 4 is still compatible with some experimental results, indicating the presence of so-called conductive channels.[16]

2. Phenomenological model of CER effect

Using our model assuming two parallel current paths (P_1 and P_2), as illustrated in Fig. 4, we got the idea that the CER effect might have a relationship with the SBH inhomogeneity. We assume that the pinched-off effect occurs because of the SS-IHG at equilibrium or quasiequilibrium states, but it does not occur completely in the case of a nonequilibrium state. Because the pinched-off effect results from a relaxation of a potential distribution between the original low SBH (Φ_{b2}) region and the surrounding high SBH (Φ_{b1}) region, it is reasonably assumed that the pinched-off effect appears after sufficient time for relaxation. Namely, we assume that the pinched-off effect is the case of the OFF state, and that the OFF state is close to the equilibrium (steady) state.

In an equilibrium or quasiequilibrium state (OFF state), the effective SBH of P_2, a domain originally having a low SBH, becomes nearly the same as the surrounding P_1, which originally has a high SBH, as the result of the pinched-off effect. In this situation, $J_{FE}(V_{a1}^*)$ and $J_{FE}(V_{a2}^*)$ are similar to each other [see Eqs. (6) and (7)] and, consequently, $R_1(V_a) \ll R_2(V_a)$ holds because of the small areal fraction of $P_2, S_1 \gg S_2$. On the other hand, in the short transient state where the pinched-off effect does not occur completely (ON state), Φ_{b2} is given approximately by the original low SBH. In this case, the relation of $\Phi_{b1} > \Phi_{b2}$ holds, the relation of $R_1(V_a) > R_2(V_a)$ can be expected, depending on the experimental conditions, as will be discussed later, and the current mainly flows through P_2.

3. Explanation of experimental results based on model

Our model explains the difference between the ON and OFF states based on SBH inhomogeneity. If our model is an appropriate one to explain the CER effect at $Pt/SrTi_{1-x}Nb_xO_3$ junctions, we have to clarify the mechanism for variations in Φ_{b2}, the effective barrier height for P_2, with a bias sequence. Namely, we have to explain the mechanism for switching between LS-IHG and SS-IHG. Here, we consider what acts as the switching trigger.

It should be noted that we could not define the critical bias inducing the switching between the ON and OFF states.[49] Namely, the threshold bias for switching between the ON and OFF states could not be clearly defined, and the magnitude of the hysteresis in an I-V curve depends on the bias sequence, i.e., the maximum forward and reverse biases. Switching from the OFF to ON state occurred when the sign of $\partial Va/\partial t$ was changed from positive to negative under the forward bias stage, and that from ON to OFF occurred when the sign of $\partial Va/\partial t$ was changed from negative to positive in the reverse bias stage. In other words, rather than the absolute value of V_a, the sign of $\partial Va/\partial t$ is likely the most important factor in the CER behavior of $Pt/SrTi_{1-x}Nb_xO_3$ junctions. We believe that time-dependent changes in the depletion layer width $[W_d(t)]$ or the space-charge density of the depletion region $[N_D(t)]$ of the Schottky barrier should be a key when we assume the presence of deep levels. As illustrated in Fig. 7 and expressed by Eq. (10), N_D varies with time when bias sweeping occurs at a certain sweeping rate, and consequently, W_d also varies with time.

When V_a is changed, a redistribution of the space charge in the depletion layer occurs, and W_d and N_D of the depletion layer reach equilibrium or quasiequilibrium values after a certain relaxation time. The narrowing of $W_d(\partial Va/\partial t > 0)$ is a process that causes the unoccupied states in the depletion layer to be occupied by the electron capture process. In contrast, the expansion of $W_d(\partial Va/\partial t < 0)$ is a process that removes electron from the occupied donor and trap states by an emission process. In general, the electron emission process takes a relatively longer relaxation time, because the emission and capture processes are endothermic and exothermic processes, respectively. Thus a nonequilibrium state with a long relaxation time tends to appear in the case of W_d expansion, as illustrated in Fig. 7. Here, a nonequilibrium state means that deep traps located above E_f remain neutral because of a low emission rate, and W_d takes a value larger than the equilibrium value to maintain charge neutrality under a certain V_a.

Because the transient behavior should be quite complicated, we were not able to construct quantitative analyses for the charge redistribution during bias sweeping in terms of the pinched-off effect. At present, we use a schematic illustration (Fig. 10) to explain the CER effect, based on the successful simulations of the I-V behaviors performed in this study. Here, we assume that the transient state appears when $W_d(\partial Va/\partial t < 0)$. Because of the long relaxation time for charge distribution in the depletion layer after the expansion of W_d, the pinched-off regime may be broken during the transient state. This may be why the ON state appears when $W_d(\partial Va/\partial t < 0)$. In contrast, the pinched-off regime is maintained for the bias sweep direction of $W_d(\partial Va/\partial t > 0)$ because of the relatively short relaxation time for the narrowing of W_d. Because no obvious relaxation behavior was seen in this study, we speculate that the relaxation time for the recovery of the pinched-off regime should be on the order of 10^4 s or more. The relaxation behavior of the ON state was reported by Hirose *et al.*[50] for $Pd/La_xSr_{1-x}TiO_3$ junctions. They studied the resistance retention behavior and, as a result, showed that the relaxation of the ON state, i.e., the gradual increase in resistance in the ON state, occurred in the time range of 10^4 s at 125 °C, with a longer time required at room temperature. Because the OFF state resistance of their sample showed less obvious relaxation behavior, their results support our speculation that the ON state is under a nonequilibrium state with a very long relaxation time.

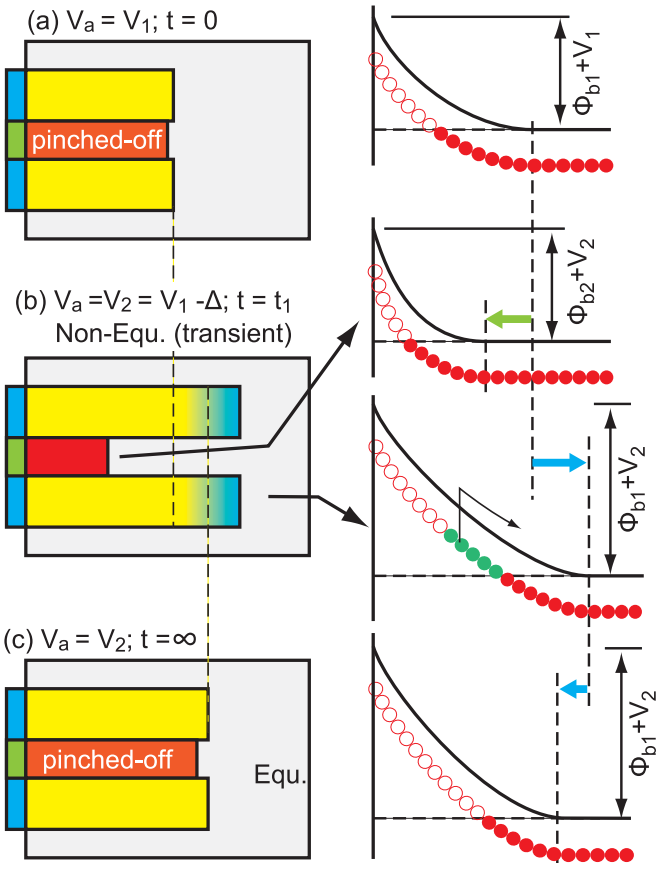

FIG. 10. (Color) Speculation about CER effect based on present results. The pinched-off regime is broken when the bias sweeps for the expansion of the depletion layer. See text for details.

VI. CONCLUSIONS

We successfully simulated experimental I-V curves for CER, which occurs in a $Pt/SrTi_{1-x}Nb_xO_3$ Schottky junction, using a model based on temperature and the electric-field dependence of the relative permittivity $\varepsilon_r(E,T)$ of $SrTi_{1-x}Nb_xO_3$ and SBH inhomogeneity. From the results of the simulations, the following conclusions were reached: (i) The anomalous temperature dependence of the I-V curves originates mainly in the field-emission current at the $Pt/SrTi_{1-x}Nb_xO_3$ interface, which is caused by the strong temperature and field dependence of $\varepsilon_r(E,T)$ at the interface. (ii) The difference between the resistance of the OFF and ON states of CER originates in the variation in the magnitude of the field-emission current, which is caused by differences in the SBH. (iii) The CER effect can be explained qualitatively on the basis of a model in which two parallel current paths coexist in the $Pt/SrTi_{1-x}Nb_xO_3$ Schottky barrier junction, which indicates that the pinched-off effect caused by the SBH inhomogeneity and the electron-occupation kinetics at a deep level of the depletion layer plays an important role in the mechanism of the CER effects.

ACKNOWLEDGMENTS

J. Li was supported by a Grant-in-Aid for the World Premier Research Institute (WPI) initiative promoted by the Ministry of Education, Culture, Sports, Science and Technology, Japan. A part of this study was supported by a Grant-in-Aid for Scientific Research from the Japan Society for the Promotion of Science.

*LI.Jianyong@nims.go.jp

†Author to whom correspondence should be addressed: OHASHI.Naoki@nims.go.jp

[1]M. Itoh, R. Wang, Y. Inaguma, T. Yamaguchi, Y-J. Shan, and T. Nakamura, Phys. Rev. Lett. **82**, 3540 (1999).

[2]K. Morito, T. Suzuki, H. Kishi, I. Sakaguchi, N. Ohashi, and H. Haneda, IEEE Trans. Ultrason. Ferroelectr. Freq. Control **54**, 267 (2007).

[3]M. Dawber, K. M. Rabe, and J. F. Scott, Rev. Mod. Phys. **77**, 1083 (2005).

[4]H. Suzuki, M. Iyori, T. Yamamoto, S. Suzuki, K. Takahashi, T. Usuki, and Y. Yoshisato, Jpn. J. Appl. Phys. **131**, 2716 (1992).

[5]T. Shimizu and H. Okushi, Appl. Phys. Lett. **67**, 1411 (1995).

[6]T. Fujii, M. Kawasaki, A. Sawa, H. Akoh, Y. Kawazoe, and Y. Tokura, Appl. Phys. Lett. **86**, 012107 (2005).

[7]T. Fujii, M. Kawasaki, A. Sawa, Y. Kawazoe, H. Akoh, and Y. Tokura, Phys. Rev. B **75**, 165101 (2007).

[8]M. C. Ni, S. M. Guo, H. F. Tian, Y. G. Zhao, and J. Q. Li, Appl. Phys. Lett. **91**, 183502 (2007).

[9]C. Park, Y. Seo, J. Jung, and D.-W. Kim, J. Appl. Phys. **103**, 054106 (2008).

[10]D. S. Shang, J. R. Sun, L. Shi, and B. G. Shen, Appl. Phys. Lett. **93**, 102106 (2008).

[11]D. S. Shang, J. R. Sun, L. Shi, Z. H. Wang, and B. G. Shen, Appl. Phys. Lett. **93**, 172119 (2008).

[12]D. S. Shang, J. R. Sun, L. Shi, J. Wang, Z. H. Wang, and B. G. Shen, Appl. Phys. Lett. **94**, 052105 (2009).

[13]J. Li, N. Ohashi, H. Okushi, T. NaKagawa, I. Sakaguchi, and H. Haneda, Mater. Sci. Eng. B **173**, 216 (2010).

[14]A. Beck, J. G. Bednorz, Ch. Gerber, C. Rossel, and D. Widmer, Appl. Phys. Lett. **77**, 139 (2000).

[15]A. Baikalov, Y. Q. Wang, B. Shen, B. Lorenz, S. Tsui, Y. Y. Sun, Y. Y. Xue, and C. W. Chu, Appl. Phys. Lett. **83**, 957 (2003).

[16]K. Szot, W. Speier, G. Bihlmayer, and R. Waser, Nat. Mater. **5**, 312 (2005).

[17]A. Sawa, F. Fujii, M. Kawasaki, and Y. Tokura, Appl. Phys. Lett. **85**, 4073 (2004).

[18]S. Seo, M. J. Lee, D. H. Seo, S. K. Choi, D.-S. Suh, Y. S. Joung, I. K. Yoo, I. S. Byun, I. R. Hwang, S. H. Kim, and B. H. Park, Appl. Phys. Lett. **86**, 093509 (2005).

[19]B. J. Choi, D. S. Jeong, S. K. Kim, C. Rohde, S. Choi, J. H. Oh, H. J. Kim, C. S. Hwang, K. Szot, R. Waser, B. Reichenberg, and S. Tiedke, J. Appl. Phys. **98**, 033715 (2005).

[20]X. Chen, N. J. Wu, J. Strozier, and A. Ignatiev, Appl. Phys. Lett. **87**, 233506 (2005).

[21]D. S. Shang, Q. Wang, L. D. Chen, R. Dong, X. M. Li, and W. Q. Zhang, Phys. Rev. B **73**, 245427 (2006).

[22]D. C. Kim, S. Seo, S. E. Ahn, D.-S. Suh, M. J. Lee, B.-H. Park, I. K. Yoo, I. G. Baek, H.-J. Kim, E. K. Yim, J. E. Lee, S. O. Park, H. S. Kim, U-In Chung, J. T. Moon, and B. I. Ryu, Appl. Phys. Lett. **88**, 202102 (2006).

[23]Y. Tokunaga, Y. Kaneko, J. P. He, T. Arima, A. Sawa, T. Fujii, M. Kawasaki, and Y. Tokura, Appl. Phys. Lett. **88**, 223507 (2006).

[24]A. Chen, S. Haddad, Y. C. Wu, Z. Lan, T. N. Fang, and S. Kara, Appl. Phys. Lett. **91**, 123517 (2007).

[25]M. C. Ni, S. M. Guo, H. F. Tian, Y. G. Zhao, and J. Q. Li, Appl. Phys. Lett. **91**, 183502 (2007).

[26]I. H. Inoue, S. Yasuda, H. Akinaga, and H. Takagi, Phys. Rev. B **77**, 035105 (2008).

[27]W. W. Zhuang, W. Pan, B. D. Ulrich, J. J. Lee, L. Stecker, A. Burmaster, D. R. Evans, S. T. Hsu, M. Tajiri, A. Shimaoka, K. Inoue, T. Naka, N. Awaya, K. Saiyama, Y. Wang, S. Q. Liu, N. J. Wu, and A. Iganatiev, Tech. Dig. Int. Electron Devices Meet. 193 (2002).

[28]I. G. Baek, M. S. Lee, S. Seo, M. J. Lee, D. H. Deo, D.-S. Suh, J. C. Park, S. O. Park, H. S. Kim, I. K. Yoo, U.-in Chung, and J. T. Moon, Tech. Dig. Int. Electron Devices Meet. 587 (2004).

[29]A. Chen, S. Haddad, Y. C. Wu, T. N. Fang, Z. Lan, S. Avanzino, S. Pangrle, M. Buynoski, M. Ratheor, W. Cai, N. Tripsas, C. Bll, M. VanBuskirt, and M. Taguchi, Tech. Dig. Int. Electron Devices Meet. 765 (2005).

[30]I. Ohdamari and K. N. Tu, J. Appl. Phys. **51**, 3735 (1980).

[31]J. L. Freeouf, T. N. Jackson, S. E. Laux, and J. M. Woodall, Appl. Phys. Lett. **40**, 634 (1982).

[32]M. V. Schneider, A. Y. Cho, E. Kolberg, and H. Zirath, Appl. Phys. Lett. **43**, 558 (1983).

[33]H. H. Guttier and J. H. Werner, Appl. Phys. Lett. **56**, 1113 (1990).

[34]R. T. Tung, Appl. Phys. Lett. **58**, 2821 (1991).

[35]R. T. Tung, Phys. Rev. B **45**, 13509 (1992).

[36]E. Dobrocka and J. Osvald, Appl. Phys. Lett. **65**, 575 (1994).

[37]W. Ramadan, S. B. Ogale, S. Dhar, L. F. Fu, S. R. Shinde, D. C. Kundaliya, M. S. R. Rao, N. D. Browning, and T. Venkatesan, Phys. Rev. B **72**, 205333 (2005).

[38]R. A. van der Berg, P. W. M. Blom, J. F. M. Cillessen, and R. M. Wolf, Appl. Phys. Lett. **66**, 697 (1995).

[39]S. Suzuki, T. Yamamoto, H. Suzuki, K. Kawaguchi, K. Takahashi, and Y. Yoshisato, J. Appl. Phys. **81**, 6830 (1997).

[40]T. Yamamoto, S. Suzuki, K. Kawaguchi, and K. Takahashi, Jpn. J. Appl. Phys. **37**, 4787 (1998).

[41]T. Susaki, Y. Kozuka, Y. Tateyama, and H. Y. Hwang, Phys. Rev. B **76**, 155110 (2007).

[42]S. M. Sze, *Physics of Semiconductor Devices*, 2nd ed. (John Wiley & Sons, New York, 1981).

[43]S. J. Fonash, Solid-State Electron. **15**, 783 (1972).

[44]Z. Sroubek, Phys. Rev. B **2**, 3170 (1970).

[45]W. A. Feil and B. W. Wessels, J. Appl. Phys. **74**, 3927 (1993).

[46]M. Sugiura, K. Uragou, M. Tachiki, and T. Kobayashi, J. Appl. Phys. **90**, 187 (2001).

[47]I. P. Raevski, S. M. Maksimov, A. V. Fisenko, S. A. Prosandeyev, I. A. Osipenko, and P. F. Tarasenko, J. Phys.: Condens. Matter **10**, 8015 (1998).

[48]R. Schafranek, S. Payan, M. Maglione, and A. Klein1, Phys. Rev. B **77**, 195310 (2008).

[49]See supplemental material at [http://link.aps.org/supplemental/10.1103/PhysRevB.83.125317] for "the bias sequence dependence of CER behavior".

[50]S. Hirose, A. Nakayama, H. Niimi, K. Kageyama, and H. Takagi, J. Appl. Phys. **104**, 053712 (2008).